Research Article

# Simple methods for estimating the performance and specification of optical components with anisotropic mid-spatial frequency surface errors

HAMIDREZA ARYAN, 1,2 D GLENN D. BOREMAN, 1,2 AND THOMAS J. SULESKI1,2,\*

**Abstract:** Specification and tolerancing of surfaces with mid-spatial frequency (MSF) errors are challenging and require new tools to augment simple surface statistics to better represent the structured characteristics of these errors. A novel surface specification method is developed by considering the structured and anisotropic nature of MSF errors and their impact on the modulation transfer function (MTF). The result is an intuitive plot of bandlimited RMS error values in polar coordinates which contains the surface error anisotropy information and enables an easy to understand acceptance criterion. Methods, application examples, and the connection of this surface specification approach to the MTF are discussed.

© 2019 Optical Society of America under the terms of the OSA Open Access Publishing Agreement

#### Introduction

Mid-Spatial Frequency (MSF) surface errors are found between low-spatial frequency 'form' errors, and high-spatial frequency 'roughness' errors generally modeled with scattering theory [1–3]. MSF errors are inherent to deterministic sub-aperture fabrication techniques [4–11] and can appear on the surface with different structured signatures (e.g. turned, milled, spiral) arising from the manufacturing method. Pseudo-random toolpaths [7] can provide a means to reduce the impacts of MSF errors. While 'roughness' errors are often random in distribution and scatter the light at large angles, MSF errors can be more structured and diffract the light at angles small enough to directly illuminate the image plane [12].

From an optical characterization perspective, early statistical approaches and models for studying the impact of MSF errors required small perturbations, and errors were assumed to be random with no structured spatial frequencies in the Power Spectral Density (PSD) [13]. Marioge and Slansky [14], and more recently Tamkin [15,16] considered the impacts of structured MSF errors on optical performance. We recently published on characterization of the impacts of anisotropic MSF errors on the 2D modulation transfer function (2D MTF) [17,18]. The impacts of structured MSF errors, as discussed in the literature, can be complex and difficult to implement, so simple methods for estimating these impacts are desirable and of use from an engineering perspective. Youngworth and Stone [1] previously developed simple estimates for the effects of MSF errors on image quality under the assumption that the errors are isotropic. We build upon their work in this paper to provide similar tools for estimating the impacts of anisotropic MSF surface errors. We note that, for isotropic surfaces, our results converge to the estimates provided in [1].

There are multiple surface specification methods, with the root mean square (RMS) of surface height errors and Power Spectral Density (PSD) as the most common. Bandlimited RMS of surface height errors is widely used within the metrology, manufacturing, and optical design communities for specification of optical surfaces [1,2,19]. Since the RMS calculation is not

 $<sup>^{</sup>I}$ Department of Physics and Optical Science, University of North Carolina at Charlotte, Charlotte, NC

<sup>&</sup>lt;sup>2</sup>Center for Freeform Optics, University of North Carolina at Charlotte, Charlotte, NC 28223, USA \*tsuleski@uncc.edu

sensitive to the shape or distribution of data and MSF signatures may have different anisotropic characteristics, MSF errors may not be sufficiently specified by a surface RMS value; *surfaces with the same RMS error but different manufacturing signatures can have different optical performance* [20]. Surfaces that pass a required RMS specification may not yield the expected optical performance, which leads to confusion between designer and manufacturer. To overcome this issue, surfaces are often over-specified, which adds considerably to fabrication costs and cycle times. Hence, while RMS error is an effective specification for high-frequency errors [21], it is not a reliable method for MSF errors with anisotropic signatures.

Power spectral density (PSD) is another powerful method of surface specification. In optics, PSD has been used for specifying high-frequency surface errors to predict scattering properties of a surface [21–25] and has been applied to quantify the full spectrum of surface errors [26,27]. The details of the PSD calculations are outside the scope of this paper but are well covered in the literature (e.g. [28,29]). The 2D PSD retains information on surface anisotropy, but these data are not easily connected to an optical performance criterion. The more commonly used 1D PSD representation is typically averaged over an orientation (e.g. horizontal, vertical, azimuthal), which loses information on anisotropy. Therefore, current methods of PSD specification are not conducive for use with anisotropic MSF errors [20]. We note that there are other ways that we benefit from the PSD in this work. In particular, PSD bandpass filters can be effectively utilized to separate MSF errors from form and roughness, and to calculate bandlimited RMS values from the volume underneath the 2D PSD of the surface within a given band [30].

In this paper, we propose a novel surface specification method for MSF errors to address the issues identified above. We quantify *directional* bandlimited RMS errors along different surface orientations in a polar representation and demonstrate connections to optical performance through the modulation transfer function (MTF) [31]. The proposed tool helps to facilitate a simple acceptance criterion to guarantee the performance of a manufactured part, which is highly desirable but currently lacking for surfaces with anisotropic MSF errors.

In section 2, we describe the calculation methodology for the proposed surface specification. In section 3, we discuss the connection between the proposed surface specification to the MTF as an optical performance metric. Section 4 discusses methods for designers to define acceptance criteria after tolerancing. In this paper we focus on the MTF of optical components in a system and do not consider impacts of sensors or detectors.

#### 2. Methodology of polar RMS specification

MTF is an effective optical performance metric for quantifying the impacts of MSF errors. In general, a surface RMS error leads to an optical phase difference from the perfect wavefront and reduces the average MTF of the system.

In order to establish a practical specification method for anisotropic surfaces with connections to optical performance, we seek to capture the directional RMS values that cause the largest reduction in MTF. To this end, we first calculate the individual RMS errors over multiple linear cross-sections on the surface error map at a specific orientation  $\theta$ , as shown in Fig. 1. Note that this approach differs from taking the RMS over the entire error map at once. The directional calculations are repeated at different angles on the error map to capture the anisotropy. We choose to do this from 0 to  $2\pi$  (rather than 0 to  $\pi$ ) to generate a symmetric and more intuitive final plot in polar coordinates. We note that the calculation procedures must accommodate experimental data, which will normally be captured as rectangular grids through, for example, interferometric surface measurements. Processing and analyzing these data in a polar format will unavoidably require masking and interpolation, which could introduce numerical artifacts. In particular, the analysis may be sensitive to local artifacts near the edge of the aperture where the data record is shorter. This issue could be mitigated, for example, by apodization, but such an approach also removes data and could introduce other numerical errors.

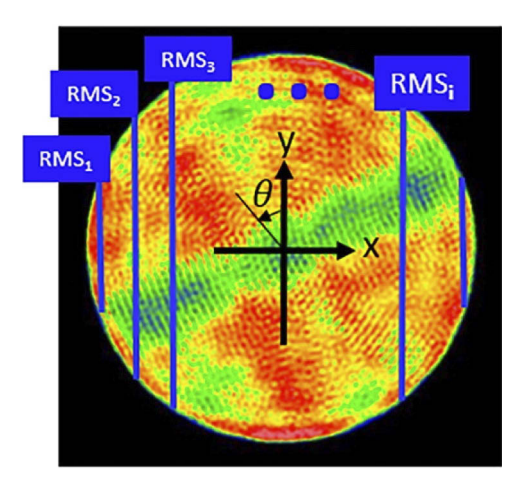


Fig. 1. Calculating directional RMS values on a surface.

We then determine the *maximum* RMS value at a given orientation and plot this value as a function of  $\theta$  in polar coordinates. The resulting *Polar RMS Plot (PRP)* captures both RMS error and anisotropy information. The word 'Polar' is chosen because results are plotted from 0 to  $2\pi$  and should not be confused with an azimuthal analysis over an error map. Calculation procedures and assumptions for the PRP are discussed in more detail in Appendix I.

To demonstrate the PRP methodology, we consider two MSF errors with the same RMS error values (53 nm), but different signatures. Figure 2 shows two diamond-machined surfaces (turned and milled) synthesized in MATLAB using the same fabrication parameters: a tool-tip radius of 1 mm and  $\Lambda$ =5 µm, where  $\Lambda$  represents feed/rev for turning and step-over for milling. A sinusoidal error with 150 nm peak to valley (PV) and 0.4 mm period was added to the resulting 'cusp-shaped' tool errors to approximate thermal drift effects from the tool chiller during manufacturing. A conventional RMS specification does not distinguish between the two surfaces, but their different anisotropy leads to different optical performance [18]. While the surface RMS values for both surfaces are equal, comparing the PRPs in Fig. 2(c) clearly shows differences between the two surfaces. We note that the directional periodic errors in Fig. 2(a) appear as distinctive peaks on the PRP in the same direction (in blue), while the PRP appears as a circle without any clear peaks (in solid red) for the rotationally symmetric errors in Fig. 2(b). We also note that for the turned texture (Fig. 2(b)) the incident light only sees a rotationally symmetric texture when on-axis; a directional texture is seen for off-axis field points or when the part is not positioned at the aperture stop.

Based on the PRP algorithm, it is expected to see peaks on the plots in the directions of the surface error periodicities. These peaks will appear wider for lower spatial frequency errors because longer spatial periods extend over several rotation angles, while higher frequency errors appear as sharper peaks. Thus, a quick look at the PRP can provide useful information about problematic surface errors.

In the next section, we discuss connections between the PRP and the MTF by making use of prior work by Youngworth and Stone in estimating the impacts of isotropic MSF errors on optical performance [1], and our recent introduction of the concept of a Minimum Modulation Curve (MMC) [17,18].

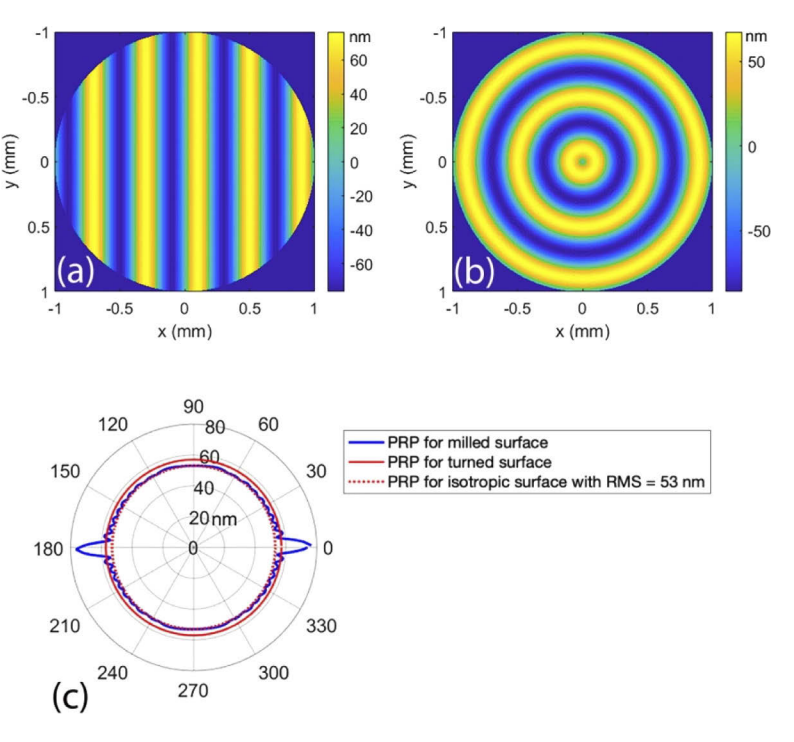


**Fig. 2.** (a) Raster-milled MSF error with RMS = 53 nm. (b) Turned MSF error with RMS = 53 nm. (c) Comparing PRPs for milled, turned, and isotropic surfaces with the same RMS.

#### 3. Connecting the PRP with the MTF

#### 3.1. Estimates of the impacts of isotropic MSF errors on optical performance

Historically, MSF errors have been primarily treated as random and isotropic. Youngworth and Stone [1] adopted a ray-based model to predict the effects of MSF errors on imaging systems at or near the diffraction limit. Despite its name, a ray-based model can include diffraction effects by tracing the rays from an object point to specific points in the exit pupil where a phase map of the wave front is constructed. The wavefront can then be used to calculate the point spread function (PSF), optical transfer function (OTF), and other performance measures. Additionally, they employed perturbation methods to estimate the additional path lengths of rays due to the presence of MSF errors, introduced concepts from statistical optics, and made multiple assumptions about the nature of the MSF errors to enable simple estimates of the impacts of these MSF errors on image quality. The end result enables the wavefront variance to be approximated for a desired object field point as:

$$\sigma_{\varphi}^2 \cong -\left(\frac{2\pi}{\lambda}\right)^2 (\Delta n)^2 \sigma^2,$$
 (1)

where  $\sigma$  is the RMS surface error over the clear aperture,  $\lambda$  is the wavelength, and  $\Delta n$  is the difference between the refractive indices of the surface and the surrounding medium [1]. Therefore, the impacts of MSF errors on Strehl ratio (*SR*) and MTF can be estimated for isotropic surfaces as:

$$SR(\sigma) = Q(\sigma) SR_{diff} = Q(\sigma)$$
 (2)

$$MTF(\sigma) = Q(\sigma)MTF_{diff}.$$
 (3)

where

$$Q(\sigma) = \exp\left[-\left(\frac{2\pi}{\lambda}\right)^2 (\Delta n)^2 \sigma^2\right],\tag{4}$$

and  $SR_{diff}$  (=1) and  $MTF_{diff}$  represent diffraction-limited performance for these two metrics.

We have introduced the idea of the PRP to better represent the impacts of anisotropic MSF errors on optical performance. In the following, we build on the work and assumptions of Youngworth and Stone [1] to demonstrate how substituting  $PRP_{max}$  (the amplitude of the largest PRP peak) instead of  $\sigma$  in Eqs. (1)–(4) connects the PRP to optical performance. Note that for an isotropic surface,  $PRP_{max} = \sigma$  and therefore our estimates converge to those from Youngworth and Stone. However, we must first briefly review key concepts of the Minimum Modulation Curve (MMC).

#### 3.2. The MMC and PRP for determining the impacts of anisotropic MSF errors

We recently introduced a new approach for 2D MTF analysis through the Minimum Modulation Curve (MMC) [17,18]. The MMC is a practical tool that summarizes key information from a 2D MTF in a more familiar 1D format. The MMC is defined as:

$$MMC(\rho) = \min_{\phi \in [0,2\pi]} \{MTF(\rho,\phi)\},\tag{5}$$

where  $MTF(\rho,\phi)$  is the MTF in polar coordinates,  $\rho$  is the radial spatial frequency, and  $\phi$  is the azimuth angle measured from the horizontal. The minimum modulation values are chosen since MTF requirements are often given as the minimum acceptable modulation at specific spatial frequencies [16]. The MMC summarizes information from all orientations and is thus suitable for analyzing the impacts of anisotropic MSF structures. To illustrate the correlation between the MMC and the MTF estimated from the PRP, we substitute  $PRP_{max}$  in place of  $\sigma$  in Eqs. (3)–(4) to obtain:

$$MTF_{PRP} = Q(PRP_{\text{max}})MTF_{diff}.$$
 (6)

As an example, we consider a 2 mm diameter f/5 PMMA (n=1.4971) lens at wavelength  $\lambda=486.1$  nm. We impose the MSF texture in Fig. 2(a) with  $\sigma=53$  nm on one side of this lens and simulate the PSF and MTF of the system via Fraunhofer diffraction theory [32]. Figure 3(a) compares the PRP of this surface (in solid blue) with the PRP of an isotropic surface (in dashed red) with the same RMS ( $\sigma=53$  nm). The blue PRP shows peaks up to  $PRP_{max}=76$  nm. As expected, the peaks are in the same direction as the periodicities of surface errors.

MTF simulation results in Fig. 3(a) confirm that the lens is not performing as predicted by Eq. (3) but does match the predictions from Eq. (6) based on the PRP. This simple example illustrates how overlooking the anisotropic nature of MSF errors could lead to an inaccurate specification. Note that both the MMC and the sagittal MTF drop below the red dashed acceptance line predicted for an isotropic MSF error. In Fig. 3(b), the PV of the sine error in Fig. 2(a) is reduced to 104 nm while keeping everything else the same. As a result, the PRP peak shrinks such that it just touches the dashed red circle representing an isotropic MSF surface error (so  $PRP_{max} = \sigma$ ), and therefore the MMC and sagittal MTF of the lens are coincident with the MTF estimation lines. In Fig. 3(c), further reduction of the sine PV to 80 nm shrinks the PRP so that  $PRP_{max} < \sigma$ , which further improves the MTF. These results suggest that the PRP can serve as an intuitive, easy to understand tool for determining an acceptance criterion.

The demonstrated relationship between PRP and MTF suggests that the PRP can provide a practical means to assign effective specifications and acceptance criteria for optical surfaces with MSF errors. The following section presents additional examples and proposes a simple method for estimating a required  $PRP_{max}$  for an optical specification.

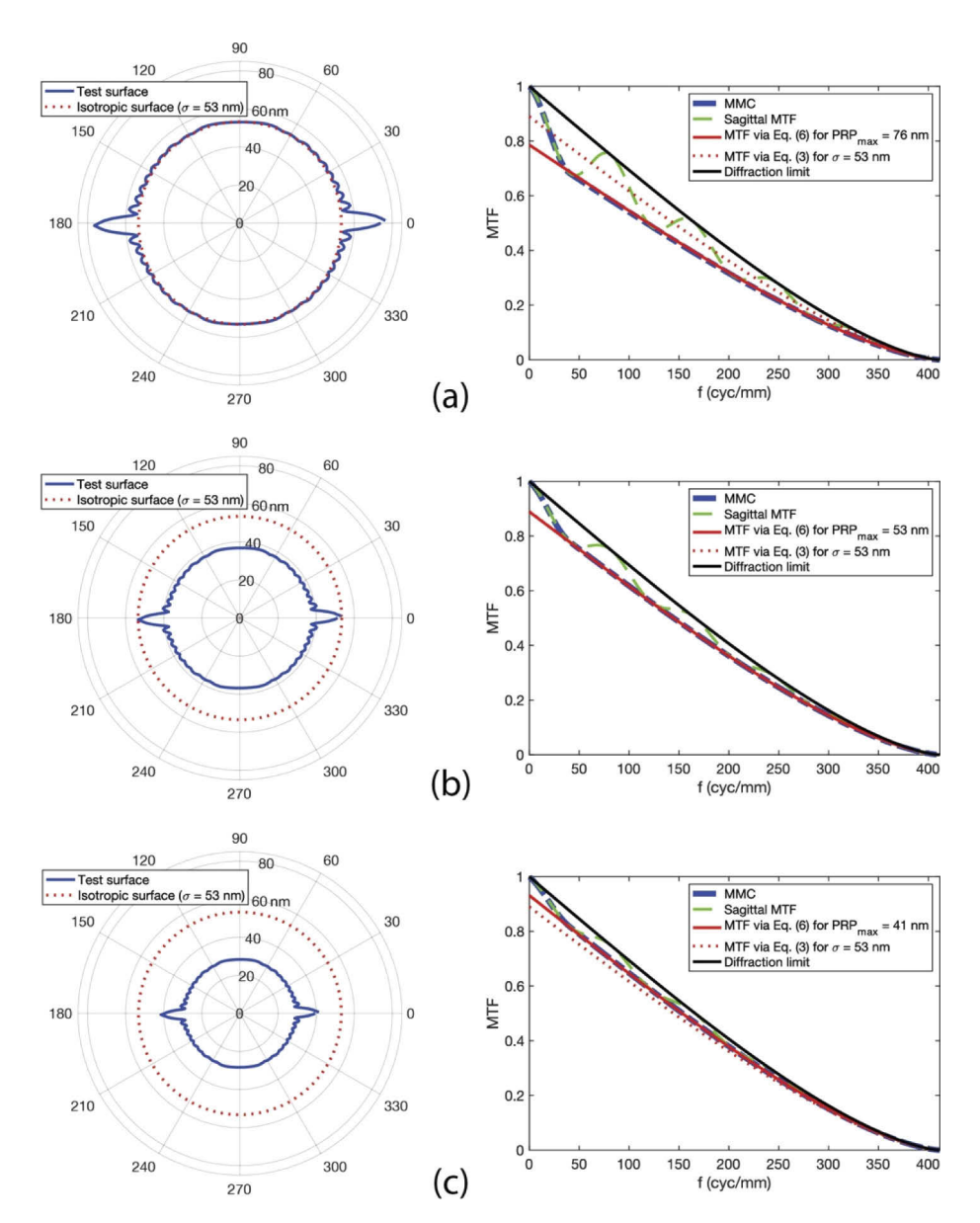


**Fig. 3.** Comparison of PRP and MTF for simple lens with surface errors of the form in Fig. 1(a) with different amplitudes. (a)  $\sigma = 53$  nm and  $PRP_{max} = 76$  nm; (b) Effects of reducing the PV of the sinusoidal error to 104 nm ( $\sigma = 37$  nm and  $PRP_{max} = 53$  nm); and (c) Effects of reducing the PV of the sinusoidal error to 80 nm ( $\sigma = 28$  nm and  $PRP_{max} = 41$  nm).

#### 4. $PRP_{max}$ as a surface specification

Optical designers are required to provide specifications on surface form, waviness (MSF errors), and roughness to manufacturers. In this section, we propose a method for calculating a  $PRP_{max}$  criterion for MSF errors after tolerancing a surface.

To this end, we again consider Eq. (2) and Eq. (4) and note that the Strehl ratio in Eq. (2) equals the multiplicative factor  $Q(\sigma)$  in Eq. (4) since  $SR_{diff} = 1$ . The SR is defined as the ratio of the central irradiance of an aberrated PSF to that of the unaberrated PSF. The SR can also be

related to the Optical Transfer Function (OTF) [33]. For small aberrations (with negligible phase transfer functions), the OTF is equivalent to the MTF and we can write:

$$SR = \frac{\iint MTF(f_x, f_y)df_xdf_y}{\iint MTF_{diff}(f_x, f_y)df_xdf_y},$$
(7)

which is the ratio of the volume under the surface of the 2D MTF of an aberrated system to the volume under the 2D MTF of a diffraction-limited system. Equation (7) can be represented in polar coordinates as:

$$SR = \frac{\iint MTF(\rho, \phi) \ \rho \ d\rho \ d\phi}{\iint MTF_{diff}(\rho, \phi) \ \rho \ d\rho \ d\phi}; \tag{8}$$

We propose to use Eq. (8) with Eq. (5) to calculate a new value SR' that is analogous to SR but based on the MMC instead of MTF. We emphasize that SR' is **not** the traditional Strehl ratio:

$$SR' = \frac{\int MMC(\rho) \ d\rho}{\int MTF_{diff}(\rho) \ d\rho} \ . \tag{9}$$

The new performance parameter SR' is connected to the maximum wavefront variance and maximum RMS surface error ( $\sigma_{max}$ ), since the MMC indicates the lowest modulation at each spatial frequency. Comparing Eq. (2), Eq. (4), and Eqs. (8)–(9) suggests that we can set:

$$SR' = \exp\left[-\left(\frac{2\pi}{\lambda}\right)^2 (\Delta n)^2 \sigma_{\text{max}}^2\right] = Q', \tag{10}$$

and thus:

$$\sigma_{\text{max}} = \frac{\lambda}{2\pi\Delta n} \sqrt{-\log_e(Q')},\tag{11}$$

where Q' is a new multiplicative factor analogous to Eq. (4) and which, considering Eq. (6), suggests that  $\sigma_{max} \approx PRP_{max}$ . Note that  $\sigma_{max}$  is calculated via the MMC where modulation equals one at zero spatial frequency, while  $PRP_{max}$  is connected to a linear estimate of the MTF through Eq. (6). As discussed below, this can cause differences between the values of  $\sigma_{max}$  and  $PRP_{max}$ , but the values are close empirically when the performance is close to diffraction-limited.

To better illustrate this point, we now consider several examples of MSF errors on the aforementioned lens used in Fig. 3 and compare the resulting MTF performances with predictions based on the methods discussed above. As shown in Fig. 4, Cases I and II correspond to simple sinusoidal signatures from raster milling and turning, respectively, while Cases III and IV contain multiple sinusoidal errors with different amplitudes and orientations. For each of these examples, we calculate the PRP from the MSF surface data and calculate the MMC following Eq. (5). We then calculate the acceptance line for MTF based on the isotropic assumptions of Youngworth and Stone [1] using Eq. (3), as well as MTF acceptance lines calculated based on  $PRP_{max}$  using Eq. (6), and based on  $\sigma_{max}$  from Eq. (11) in place of  $PRP_{max}$  in Eq. (6). The PV, period ( $\Lambda$ ), and direction ( $\theta$ ) of the sinusoidal errors on each of surfaces are listed in Table 1. The calculated surface specifications for each example are listed in Table 2, and the corresponding MSF surfaces, PRPs, and MTF comparisons are shown in Fig. 5.

We note that all four cases have the same  $\sigma$ , but do not have the same optical performance. For the rotationally symmetric example (Case II), the performance predicted by all methods is very close to that expected for an isotropic surface. However, the performance of surfaces with more anisotropy (Cases I, II, and IV) are consistently below the expectation for an isotropic surface. We also note that the MTF lines predicted via  $\sigma_{max}$  and  $PRP_{max}$  are very close and track well with the MMC.

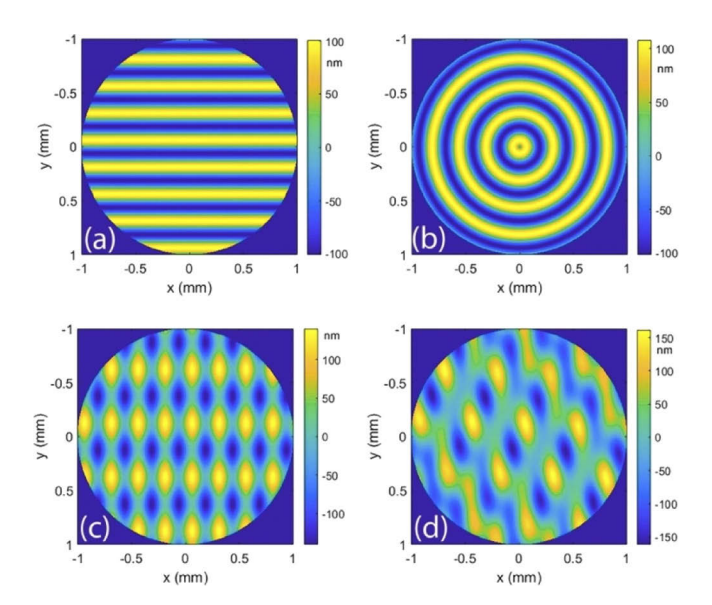


Fig. 4. Surface errors from Table 1: (a) Case I. (b) Case II. (c) Case III. (d) Case IV.

Table 1. List of sinusoidal errors for example surfaces in Fig. 4.

	PV <sub>1</sub> (nm)	$\Lambda_1 \ (mm)$	$\theta_1$ (deg)	PV <sub>2</sub> (nm)	$\Lambda_2 \ (mm)$	$\theta_2$ (deg)	PV <sub>3</sub> (nm)	$\Lambda_3 \text{ (mm)}$	$\theta_3$ (deg)
Case I	200	0.25	0	-	-	-	-	-	-
Case II	200	0.25	No	-	-	-	-	-	-
Case III	150	0.25	90	130	0.5	0	-	-	-
Case IV	100	0.25	90	75	0.5	0	150	0.4	60

Table 2. Calculated specification for example surfaces in Fig. 4.

	$\sigma$ (nm)	$\sigma_{max}$ (nm)	PRP <sub>max</sub> (nm)	Q = SR	Q' = SR'
Case I	70	100	100	0.84	0.71
Case II	70	70	74	0.84	0.84
Case III	70	93	100	0.84	0.75
Case IV	70	93	101	0.84	0.75

We now consider an additional example that demonstrates application to an experimental data set and also illustrates potential limitations of the proposed methodology. Figure 6(a) shows data from an experimental interferometric measurement of a surface created through a raster grinding process. It can be argued [2] that the low-spatial frequency sinusoidal errors in the vertical direction should be considered to be form errors, rather than MSF errors; thus, the measurement result can be thought of as a 'non-ideal' surface with residual form errors after filtering the data. Figure 6(b) shows the PRP for this experimental surface, with large, wide peaks and large PV in the vertical direction corresponding to the low-spatial frequency errors. The measured RMS  $(\sigma)$  and  $PRP_{max}$  for this surface are 7 nm and 11 nm, respectively.

For optical simulations, we impose this surface error onto a f/10 mirror with 0.418 mm clear aperture at a wavelength of  $\lambda=157$  nm. We note that  $\Delta n=2n=2$  in Eq. (4) for the reflective case in air since light reflects back into the same medium. Use of Eq. (9) and Eq. (11) results in  $\sigma_{max}=8.7$  nm. The corresponding MTF simulations for this example are for the reflective caseshown in Fig. 6(c).

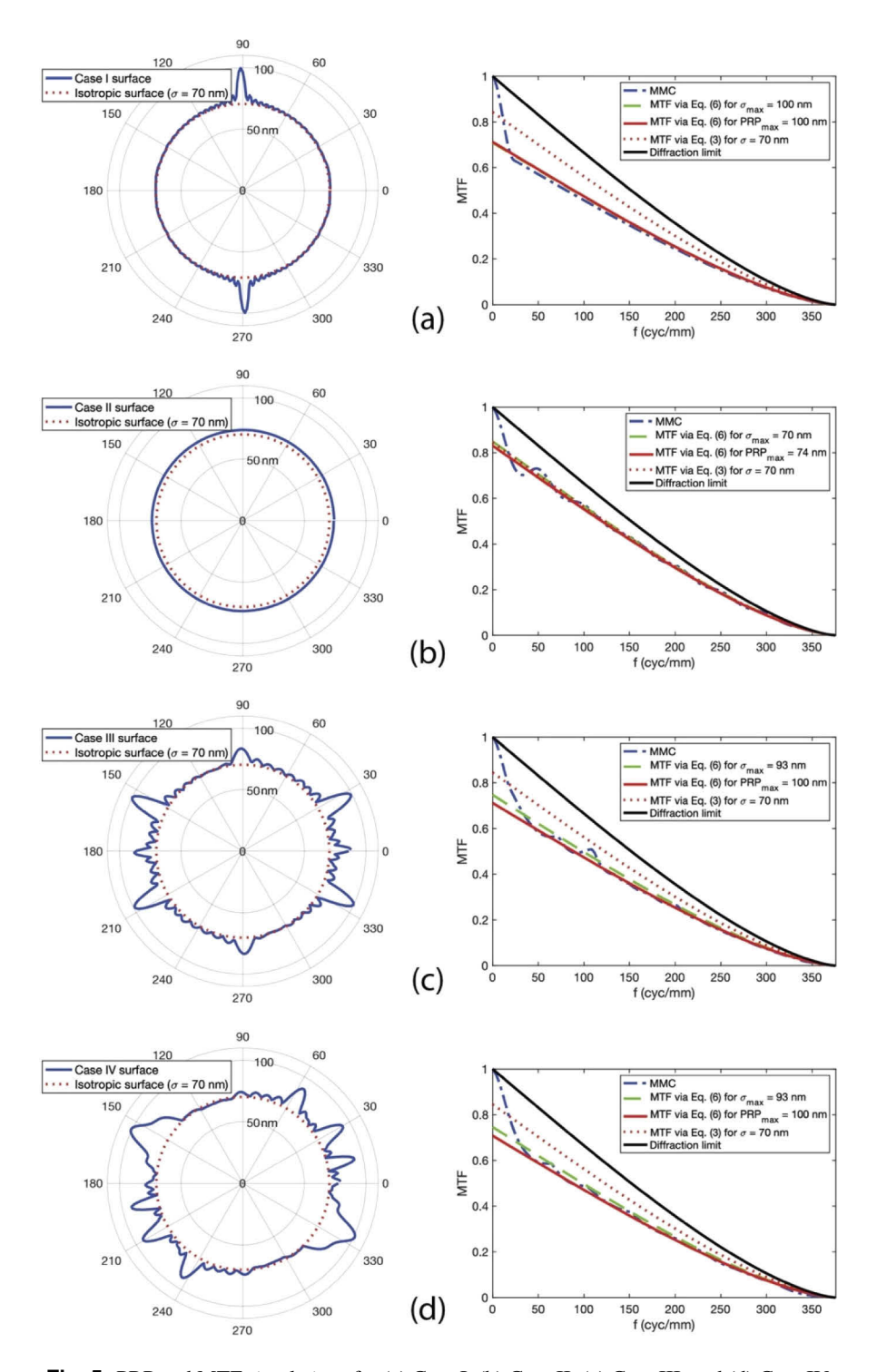
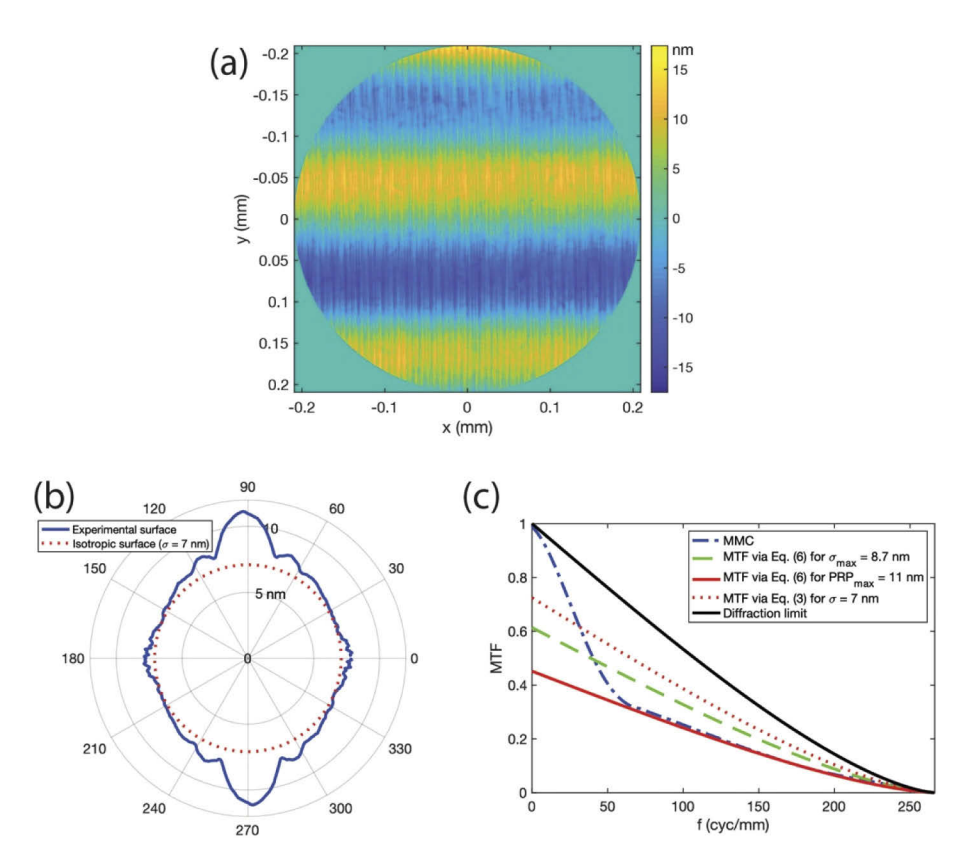


Fig. 5. PRP and MTF simulations for (a) Case I, (b) Case II, (c) Case III, and (d) Case IV.



**Fig. 6.** (a) Example of experimental surface error from raster grinding on a mirror surface, and corresponding (b) PRP, and (c) MTF calculations for system operating at  $\lambda = 157$  nm.

Multiple useful observations can be made from the simulations in Fig. 6(c). The MTF prediction from the experimentally determined  $PRP_{max}$  value from Fig. 6(b) tracks well with the MMC; the connection between the measured PRP and the MMC holds true even with the presence of the low-spatial frequency errors in the experimental surface data. However, the MTF line resulting from the calculated  $\sigma_{max}$  value shows a significant deviation from the MMC. This illustrates that the assumptions used in setting  $PRP_{max} \approx \sigma_{max}$  are not valid in the presence of low-spatial frequency errors with PV values that are large in comparison to the MSF contributions. This makes sense, as such errors lead to drops in the MMC that introduce a bias in Eq. (9), resulting in  $\sigma_{max} < PRP_{max}$ . This bias is also observable at a lesser level in Figs. 5(c) and 5(d). However, we note that the predictions using  $\sigma_{max}$  still provides better estimates than values calculated via Eq. (3) for an isotropic surface.

To conclude this section, we note that Eq. (11) provides a simple method for designers to estimate  $PRP_{max}$  as an acceptance criterion after tolerancing optical system performance based on the MMC, subject to the assumptions and limitations discussed above. For example, if the aforementioned lens in Fig. 3 is required to have an MMC above 80% of the diffraction limit at all spatial frequencies, then Q' = 0.8. For this value of Q', Eq. (11) can be used to estimate  $\sigma_{max} \approx PRP_{max} = 73$  nm. Even more simply, we assert that it would be reasonable for a designer who calculated a required value of  $\sigma$  (assuming an isotropic MSF error distribution) to provide that same numerical value as the  $PRP_{max}$  to the manufacturer as an acceptance criterion.

#### 5. Discussion and conclusion

We have proposed a novel method for specification of optical surfaces with anisotropic MSF surface errors based on the maximum RMS surface error in a given direction. Presenting the resulting data in polar coordinates results in a *Polar RMS Plot* (PRP) that enables a simple, intuitive acceptance criterion for anisotropic MSF surface errors. We have demonstrated connections between the maximum PRP value and the minimum optical modulation (MMC). The proposed methods provide a means to specify and set acceptance criteria for surfaces with anisotropic MSF errors. We note that, in the case of isotropic MSF surface errors, the proposed methods simplify to previously reported results [1]. In summary:

- The impacts of anisotropic distributions of MSF errors are captured by the MMC. The MMC can be estimated using Eq. (6) for a given  $PRP_{max}$ .
- Designers can estimate an acceptable  $PRP_{max}$  value for a surface via Eq. (11) and provide this value to manufacturers as a specification for MSF surface errors. This is in contrast to methods that provide a surface RMS value assuming isotropic error distributions and give unexpected performance results when anisotropic MSF errors are present.
- Manufacturers can use the PRP as a measurement tool and the  $PRP_{max}$  value as an acceptance criterion.

The intuitive PRP could also provide insights to manufacturers for process refinement and improvement. Since the PRP provides visual information on the orientation of surface errors and the widths of the peaks in the PRP are related to the spatial frequencies of those errors, the PRP and  $PRP_{max}$  may be useful in diagnosing processing issues that have the largest impacts on optical performance.

### Appendix I: Procedures for calculating the polar RMS plot (PRP)

- (1) Filter the desired mid-spatial frequency band using a PSD band-pass filter and save the new error map for processing.
- (2) Apply an aperture to the error map to select the analysis area.
- (3) Consider the surface height error map, H(i, j), to be an  $N_x \times N_y$  matrix. Calculate the RMS of real and non-zero values for each column of this matrix according to Fig. 1. Then pick the *maximum* RMS value between all columns.
- (4) Rotate the surface error map by a small angle  $(\Delta\theta)$ . In this paper, we chose one-degree angular increments and the nearest-neighbor interpolation method using the *imrotate.m* function in MATLAB.
- (5) Repeat Steps 3 and 4 for each angle  $(\theta)$  across the desired angular range. We chose to perform this calculation from 0 to  $2\pi$  to enable an intuitive, symmetric final plot.
- (6) Plot the maximum RMS value captured at each rotation angle of the surface error map with respect to each angle in polar coordinates.

Depending on the shape of incident beam footprint on the part, the user can apply a circular or rectangular aperture to the error map to select the analysis area. Although we have used a circular aperture in our calculations, the choice of aperture has not shown an impact on the overall PRP properties or its connection to optical performance. Choice of a circular aperture is

straightforward, but to apply a rectangular aperture, it is safer to crop down the surface area to  $N/\sqrt{2}$  size, where  $N = \min\{N_x, N_y\}$ . This is suggested to avoid any noise leakage from the edges into the PRP data caused by the required matrix rotations in step (4).

The PRP resolution depends on the choice of angular increment  $(\Delta\theta)$  in rotating the surface error map. Surface resolution and the accuracy of the interpolation method used for rotating the surface matrix are other limiting factors. Similar to other surface specification methods, it is a good practice to mask large localized amplitude spikes within measured data to avoid unnecessary over-specification.

It is also important to remember that the position and diameter of the analysis on a measured part should be chosen based on the expected beam footprint within the design. It could be necessary to specify a part at different field angles. This helps to establish an effective specification connected to optical performance.

#### Funding

National Science FoundationI/UCRC Center for Freeform Optics (IIP-1338877, IIP-1338898, IIP-1822026, IIP-1822049).

#### Acknowledgments

Portions of this work were presented at the 2019 OSA Optical Design and Fabrication Congress in "Specification of Optical Surfaces with Anisotropic Mid-Spatial Frequency Errors" [34]. The authors would like to acknowledge helpful discussions with Dr. Chris Evans and Dr. Brigid Mullany from UNC Charlotte, and Dr. Miguel Alonso and Kevin Liang from the University of Rochester. We also would like to thank Raj Shanmugam from UNC Charlotte for providing experimental data.

#### References

- R. N. Youngworth and B. D. Stone, "Simple estimates for the effects of mid-spatial frequency surface errors on image quality," Appl. Opt. 39(13), 2198–2209 (2000).
- D. M. Aikens, J. E. DeGroote, and R. N. Youngworth, "Specification and Control of Mid-Spatial Frequency Wavefront Errors in Optical Systems," in Frontiers in Optics 2008/Laser Science XXIV/Plasmonics and Metamaterials/Optical Fabrication and Testing, OSA Technical Digest (CD) (Optical Society of America, 2008), paper OTuA1.
- L. L. Deck and C. Evans, "High performance Fizeau and scanning white-light interferometers for mid-spatial frequency optical testing of free-form optics," Proc. SPIE 5921, 59210A (2005).
- H. Aryan, K. Liang, M. A. Alonso, and T. J. Suleski, "Predictive models for the Strehl ratio of diamond-machined optics," Appl. Opt. 58(12), 3272–3276 (2019).
- R. Rhorer and C. Evans, "Fabrication of optics by diamond turning," in *Handbook of Optics, Third Edition Volume II: Design, Fabrication and Testing, Sources and Detectors, Radiometry and Photometry*, M. Bass, C. DeCusatis, J. Enoch, V. Lakshminarayanan, G. Li, C. Macdonald, V. Mahajan, and E. Van Stryland, eds. (McGraw-Hill, 2009), Chap. 10.
- W. B. Lee, C. F. Cheung, and S. To, "Material-induced Vibration in Single Point Diamond Turning," in *Machining Dynamics*, K. Cheng, ed. (Springer, 2009), Chap. 9.
- C. R. Dunn and D. D. Walker, "Pseudo-random tool paths for CNC sub-aperture polishing and other applications," Opt. Express 16(23), 18942–18949 (2008).
- 8. A. Sohn, L. Lamonds, and K. Garrard, "Modeling of Vibration in Single-Point Diamond Turning," in *Proceedings of the American Society of Precision Engineering* (ASPE, 2006), pp. 15–20.
- 9. G. W. Forbes, "Never-ending struggles with mid-spatial frequencies," Proc. SPIE 9525, 95251B (2015).
- Z. Hosseinimakarem, H. Aryan, A. Davies, and C. Evans, "Considering a Zernike polynomial representation for spatial frequency content of optical surfaces," in *Imaging and Applied Optics 2015, OSA Technical Digest (online)* (Optical Society of America, 2015), paper FT2B.2.
- 11. J. A. Shultz, H. Aryan, J. D. Owen, M. A. Davies, and T. J. Suleski, "Impacts of sub-aperture manufacturing techniques on the performance of freeform optics," in *Proceedings ASPE/ASPEN Spring Topical Meeting: Manufacture and Metrology of Structured and Freeform Surfaces for Functional Applications* (2017), paper 0061.
- J. Filhaber, "Mid-spatial-frequency errors: the hidden culprit of poor optical performance," Laser Focus World 49(8), 32 (2013).
- E. L. Church and J. M. Zavada, "Residual surface roughness of diamond-turned optics," Appl. Opt. 14(8), 1788–1795 (1975).

- 14. J. P. Marioge and S. Slansky, "Effect of figure and waviness on image quality," J. Opt. 14(4), 189-198 (1983).
- J. M. Tamkin, T. D. Milster, and W. Dallas, "Theory of modulation transfer function artifacts due to mid-spatial-frequency errors and its application to optical tolerancing," Appl. Opt. 49(25), 4825–4835 (2010).
- 16. J. M. Tamkin, "A Study of Image Artifacts Caused by Structured Mid-spatial Frequency Fabrication Errors on Optical Surfaces", Dissertation, The University of Arizona, (2010).
- 17. H. Aryan and T. J. Suleski, "Non-directional modulation transfer function for optical surfaces with asymmetric mid-spatial frequency errors," in *Optical Design and Fabrication 2019 (Freeform, OFT), OSA Technical Digest (online)* (Optical Society of America, 2019), paper OT1A.2.
- H. Aryan, G. D. Boreman, and T. J. Suleski, "The Minimum Modulation Curve as a tool for specifying optical performance: application to surfaces with mid-spatial frequency errors," Opt. Express 27(18), 25551–25559 (2019).
- ISO 10110 Optics and photonics Preparation of drawings for optical elements and systems. Part 8: Surface texture; roughness and waviness (2010).
- H. Aryan, C. J. Evans, and T. J. Suleski, "On the Use of ISO 10110-8 for Specification of Optical Surfaces with Mid-Spatial Frequency Errors," in *Optical Design and Fabrication 2017 (Freeform, IODC, OFT), OSA Technical Digest (online)* (Optical Society of America, 2017), paper OW4B.2.
- 21. J. C. Stover, Optical Scattering: Measurement and Analysis, 2nd Edition (SPIE, 1995), Chap. 2.
- J. E. Harvey, "X-ray optics," in Handbook of Optics, 2nd Edition Volume II: Devices, Measurements, and Properties, M. Bass, E. Van Stryland, D. R. Williams, and W. L. Wolfe, eds. (McGraw-Hill, 1995), Chap. 11.
- J. M. Bennett and L. Mattsson, Introduction to Surface Roughness and Scattering, 2nd Edition (Optical Society of America, 1999).
- J. M. Elson and J. M. Bennett, "Calculation of the power spectral density from surface profile data," Appl. Opt. 34(1), 201–208 (1995).
- A. Duparré, J. Ferre-Borrull, S. Gliech, G. Notni, J. Steinert, and J. Bennett, "Surface characterization techniques for determining the root-mean-square roughness and power spectral densities of optical components," Appl. Opt. 41(1), 154–171 (2002).
- D. M. Aikens, C. R. Wolfe, and J. K. Lawson, "The use of Power Spectral Density (PSD) functions in specifying optics for the National Ignition Facility," Proc. SPIE 2576, 281–292 (1995).
- 27. J. K. Lawson, C. R. Wolfe, K. R. Manes, J. B. Trenholme, D. M. Aikens, and R. E. English Jr., "Specification of optical components using the power spectral density function," Proc. SPIE 2536, 38–50 (1995).
- R. N. Youngworth, B. B. Gallagher, and B. L. Stamper, "An overview of power spectral density (PSD) calculations," Proc. SPIE 5869, 58690U (2005).
- E. Sidick, "Power spectral density specification and analysis of large optical surfaces," Proc. SPIE 7390, 73900L (2009).
- 30. Zygo Corp., "Data processing: Using the filter PSD plot," in Mx Help (Zygo, 2015).
- 31. G. Boreman, Modulation Transfer Function in Optical and Electro-Optical Systems (SPIE, 2001), Chap. 1.
- 32. J. W. Goodman, Introduction to Fourier Optics (Roberts and Company, 2005), Chap. 5.
- 33. J. W. Goodman, Introduction to Fourier Optics (Roberts and Company, 2005), Chap. 6.
- 34. H. Aryan and T. J. Suleski, "Specification of Optical Surfaces with Anisotropic Mid-Spatial Frequency Errors," in Optical Design and Fabrication 2019 (Freeform, IODC, OFT), OSA Technical Digest (online) (Optical Society of America, 2019), paper OM4A.5.